Measurements of aerosol dimensional distributions and microphysical characteristics: A comparison between Raman lidar and airborne sensors

P. Di Girolamo[1], B. De Rosa[1,2], D. Summa[1,2], N. Franco[1], I. Veselovskii[3], E. Freney[4]

[1]Scuola di Ingegneria, Università degli Studi della Basilicata, Potenza, 85100, Italy

[2] Istituto di Metodologie Ambientali, Consiglio Nazionale delle Ricerche, Tito Scalo (PZ), Italy

[3]Prokhorov General Physics Institute of the Russian Academy of Sciences, Moscow, Russia

[4]Laboratoire de Météorologie Physique, CNRS/Université Blaise Pascal, Clermont-Ferrand, France

Corresponding author: Paolo Di Girolamo (paolo.digirolamo@unibas.it)

Key Points:

- Aerosol physical and chemical characteristics from a three-wavelength Raman lidar and airborne microphysical and chemical sensors
- A retrieval approach based on Tikhonov regularization is applied to lidar measurements to infer aerosol size and microphysical properties
- Ensemble back-trajectory modeling and measurements combined to determine aerosol types and origins and their source–receptor relationships

Abstract

This manuscript compares aerosol size distributions and microphysical property measurements from the Raman lidar BASIL and from aircraft sensors during HyMeX-SOP1. The attention was focused on a measurement session on 02 October 2012, with BASIL measurements revealing the presence of a lower aerosol layer extending up to 3.3 km and an elevated layer with extending from 3.6 km to 4.6 km. Aerosol size distributions and microphysical characteristics were determined from three-wavelength particle backscattering and extinction profile measurements through a retrieval approach based on Tikhonov regularization.

A good agreement is found between BASIL retrievals and the microphysical sensors' measurements for all considered aerosol dimensional and microphysical characteristics. Specifically, BASIL and in-situ volume concentration values are 1-3.5 mm^3cm^{-3} in the lower layer and 2-4 mm^3cm^{-3} in the upper layer. Furthermore, effective radius values from BASIL and the in-situ sensors' measurements are in the range 0.2-0.6 m both in the lower and upper layer. Particle size distributions were determined at 2.2, 2.8, 4 and 4.3 km, with again a good

agreement between the Raman lidar and the microphysical sensors throughout the considered height interval. These results, in combination with Lagrangian back-trajectory analyses and chemical composition measurements, indicate that aerosols below 3 km were possibly originated by forest fires in North America or by anthropogenic activities in North-Eastern Europe, while aerosols above 3 km were originated over the North Atlantic and presumably include both a marine and an organic component. This interpretation is compatible with the lidar retrieved profiles of particle complex refractive index.

1 Introduction

Aerosols are suspended particles including a large number of species, such as minerals, sea salt, dust, nitrates, sulphates, water and carbon, which may greatly vary in size (Bonsang et al., 1992; Leck and Bigg, 2005a; 2005b). Aerosols are directly injected in the atmosphere as particles (primary aerosols) or may form in it through chemical reactions involving gaseous species (secondary aerosols). While primary aerosols are of all sizes, secondary aerosols are primarily in the sub-micron-meter size range (< 0.1 m).

Carbonaceous aerosols, especially in urban areas, may be composed of black carbon or include organic components (Mansfield et al., 1991; Rogge et al., 1993; Rogge et al., 1993; Andrews et al., 2000; Turpin e t al., 2000),which are the primary components of polluted aerosols expelled by vehicles (Fraser et al., 2002) and heating. Furthermore, urban aerosols may contain sulphates, with $SO_2$from anthropogenic sources acting as a precursor. Sources of SO_2 and their magnitude and distribution are reasonable well known (among others, Lelieveld et al.1997), with estimates differing by 20 to 30%.

Nitrate is another important component of urban aerosols, its presence being closely related to the abundance of ammonium and sulphate (Bauer et al., 2007). If ammonia is present is sufficiently high concentrations to neutralise sulphuric acid, nitrate can form small and radiatively active particles. In recent years the role of nitrate has been investigated in detail to assess its role in aerosol radiative properties. The global amount of nitrate aerosols from human activities is 0.4 Tg and it is responsible for$\sim$ 2% of the overall direct aerosol forcing (Bauer et al., 2007), while the contribution from natural sources is 0.24Tg (Bauer et al., 2007).

Maritime aerosols are particularly important as sea water covers approximately 70 % of the Earth surface, and they largely contribute to the global aerosol burden. Furthermore, marine aerosols may modify the reflectance and lifetime of marine stratiform clouds. Over remote oceans, aerosols primarily composed include sea salt and sulphates, the latter being the result of the oxidation of biogenic dimethyl sulphide and organic particles. The main precursor of marine sulphate aerosols is biogenic dimethyl sulphide from biogenic sources, primarily marine plankton. Maritime aerosols in high wind speed regions are primarily

composed of sea salt, while sulphates are the predominant component in biologically active regions (Andreae et al., 1995; Falkowski et al., 1992).

Increased levels of organic carbon (OC) were recently reported from marine aerosol samples, with particles being characterized by smaller radii compared to normal marine aerosols. Analyses of their chemical composition indicated that most part of submicron marine aerosol component observed over productive ocean waters are organic (O'Dowd et al., 2004; Facchini et., 2008; Keene et al., 2007; Zorn et., 2008). Nitrate aerosols are also present in the marine environment and their abundance is primarily linked to ocean ecosystem productivity, with nitrate having the possibility to deposit on larger sea salt aerosols (Bassett and Seinfeld, 1984; Murphy and Thomson, 1997; Gard et al., 1998). Particles in the coarse mode behave as more inefficient scatters, this ultimately translating into a reduced radiative effect of nitrate aerosols (Zhang et al., 2000; Li-Jones and Prospero, 1998).

Tropospheric aerosols represent a primary component of the Earth's radiation budget. Atmospheric scattering and absorption of both solar and planetary radiation are strongly dependent on aerosol concentration (Twomey, 1977; Albrecht, 1989; Charlson et al., 1992; IPCC, 2007). Additionally, aerosol concentrations may influence nucleation and cloud microphysical processes.

Aerosol mass and particle concentrations are characterized by a high space and time variability. Consequently, the quantification of aerosol forcing on the radiative budget is affected by larger uncertainties than the quantification of greenhouse gases forcing. This is also caused by the shorter lifetime of atmospheric aerosols as compared to important greenhouse gases. For the purpose of quantitatively estimate aerosol radiative forcing, spatially and temporally resolved information on atmospheric aerosol chemical, size, microphysical and radiative properties are necessary (Rap, 2013; Boucher et al., 2013). Among the size and microphysical aerosol characteristics: real and imaginary part of the refractive index, volume concentration, effective radius and particle size distribution.

Vertical profiles of aerosol size and microphysical properties can be measured by few techniques. Airborne in situ sensors represent an effective source of data. However, their application is costly and complex, and this ultimately translates into a limited use of such sensors. Remote sensing techniques, as multi-wavelength Raman lidars, are potentially well suited, but performance needs to be validated based on the comparison with independent measurements.

Aerosol optical properties are the longest measured parameters by, with pioneering measurements available since the nineteen-sixties (Fiocco and Grams, 1964; Elterman, 1966). Initially only single-wavelength particle backscattering coefficient profile measurements were possible. Particle backscattering coefficient profiles are determined from the single-wavelength elastic signals through different approaches (Klett, 1981; Klett 1985; Fernald, 1984; Di Girolamo et al., 1995; Di Girolamo et al., 1999). Later particle extinction coefficient profile measurements became possible thanks to the acquired ability to measure

Raman backscatter lidar signals from N_2 and O_2 molecules (Ansmann et al., 1990; Ansmann et al., 1992). A variety of authors have recently demonstrated the capability to determine aerosol dimensional and microphysical parameters from multi-wavelength Raman lidar measurements of the aerosol backscattering and extinction coefficient and depolarization ratio profiles (Müller et al., 1999; Müller et al., 2007; Freudhenthaler et al., 2009; Veselovskii et al., 2002; Veselovskii et al. 2010; Veselovskii et al. 2018). These profiles can be combined with co-located atmospheric humidity and temperature profiles with the purpose to characterize aerosol–cloud interaction mechanisms (Wulfmeyer et al., 2005; Di Girolamo et al., 2008; Di Girolamo et al., 2018).

The Raman lidar system BASIL, developed by University of Basilicata, provides three-wavelength Raman lidar measurements of aerosol optical properties, with high accuracy and high vertical and temporal resolution, to be used for the determination of particle size distributions and microphysical properties (Veselovskii et al., 2010; Di Girolamo et al., 2012). In the present paper aerosol size distributions and microphysical parameters determined from three-wavelength particle backscattering and extinction profile measurements are compared with measurements by microphysical sensors hosted by the French research aircraft ATR42. Reported measurements, collected during the First Special Observation Period (SOP1) of the Hydrological Cycle in the Mediterranean Experiment (HyMeX), represent a unique dataset to verify the accuracy and reliability of the considered inversion approaches in inferring particle size and microphysical properties. A retrieval approach based on Tikhonov regularization has been applied to multi-wavelength BASIL measurements.

HyMeX-SOP1 took place in the North-Western Mediterranean basin in September–November 2012. The experiment involved a large ensemble of instruments distributed on a variety of measurement sites. In the frame of this field deployment, BASIL was collated in an observational site in a coastal area in Southern France facing the Gulf of Lion (Candillargues, Lat: 43.61° N, Long: 4.07° E, Elev: 1 m). During HyMeX-SOP1, the ATR42 was hosting several sensors for the study of turbulence and aerosol/cloud microphysical processes. The research aircraft carried out approximately 60 flight hours, with 8 of these being funded by a specific project of the European Commission 7^{th} Framework Program (EUFAR, project WaLiTemp). The aircraft flight pattern included vertical spirals centred approximately 20 km East of the Raman lidar site, because of the imposed restrictions to air-traffic, finally displaced.

In the present paper a number of aerosol size and microphysical properties, namely volume concentration, effective radius and real and imaginary part of the refractive index, determined from three-wavelength particle backscattering and extinction profiles measured a Raman lidar, are compared with in-situ measurements, as well as with literature data.

The paper outline is as follows. Section 2 illustrates the different instruments considered in the research effort. Section 3 illustrates the methodology considered to infer aerosol size distributions and microphysical parameters from the

three-wavelength particle backscattering and extinction coefficient profile measurements. Section 4 illustrates the results from the comparison of the retrievals from the multi-wavelength Raman lidar measurements and the in-situ sensors' measurements. Section 5 summarizes the results and gives some perspectives for future follow-on activities.

2 Instruments

2.1 BASIL

The lidar includes a Nd:YAG laser source equipped with frequency doubling and tripling crystals and emitting pulses at 1064, 532 and 354.7 nm, with a frequency rate of 20 Hz. The receiver in developed around a Newtonian telescope, with a primary mirror diameter of 0.45-m. Two 0.05-m diameter lenses are also included in the receiver for the collection of the elastic echoes at 532 and 1064 nm.

BASIL can perform accurate measurements of the vertical profiles of atmospheric water vapour and temperature, with high time and vertical resolution, both day and night, based on the exploitation of the vibrational and rotational Raman lidar techniques, respectively, in the ultraviolet (Di Girolamo et al., 2004; 2006; 2009; De Rosa et al, 2018; De Rosa et al, 2020). In addition to water vapour and temperature, BASIL also carries out vertical profile measurements of the particle backscattering coefficient at 354.7, 532 nm and 1064 (referred to in the following as *3*), the particle extinction coefficient at 354.7 nm and 532 (referred to in the following as *2*), and particle depolarization at 354.7 and 532 nm. These measurements are used in the present paper to determine particle dimensional distributions and microphysical properties. In addition to HyMeX-SOP1, the Raman lidar BASIL participated in several other international field deployments (among others, Di Girolamo et al., 2012b; Di Girolamo et al., 2018; Di Girolamo et al., 2020; Summa et al., 2018; De Rosa et al, 2018).

2.2 Instruments on board ATR-42 aircraft

Several microphysical and chemical sensors with in situ measurement capability are included in the instrumental ensemble hosted by the ATR-42 atmospheric research aircraft, operated by SAFIRE (Service des Avions Français Instrumentés pour la Recherche en Environnement). During HyMeX-SOP1, the research aircraft was based at Montpellier airport. 28 flights were carried out between 11 September and 4 November 2012 .

An optical particle counter (hereafter OPC), produced by GRIMM Aerosol Technik GmbH, provides measurements of the aerosol dimensional distributions in the size range 350–2500 nm (Heim et al., 2008). A 683-nm laser beam emitted by a diode laser is radiated over the aerosol sample and the scattered radiation is detected by a photo-sensor module. The sensor includes 31 size bins. The total number concentration is derived by integrating particle number concen-

tration over the above specified size range. The OPC was specifically designed for airborne exploitation (Sullivan et al., 2014).

A Scanning Mobility Particle Sizer (hereafter SMPS) measures the dimensional distributions of aerosol particles in the size range 20– 485 nm. The SMPS operation principle relies the measurement of the accumulated charge on a specific target resulting from the aerosols being first charged and then subjected to an electrical field (Crumeyrolle et al., 2010). The combined use of the measurements from the SMPS and the OPC allows to determine particle size distributions within the size range 20 nm – 2.5 m. The upper limit of the in-.situ measurements does not allow the characterization of large and giant aerosols, which represent a substantial fraction of marine aerosols. This upper size limit is not present in the multi-wavelength lidar measurements at 355, 532 and 1064 nm (3 +2), whose retrieval capability can properly reproduce particle size distributions in the radii range 0.075–10 m (Veselovski et al., 2012).

An Aerosol Mass Spectrometer (Drewnick et al., 2005; Canagaratna et al., 2007) was also used to quantify species as ammonium sulphate and bisulphate, ammonium chloride, ammonium nitrate, and organic compounds. This is the primary instrumentation considered in this research effort for the determination of the aerosol particles composition. The information on black carbon is missing.

A specific flight pattern was conceived for the purposes of the EUFAR project "WaLiTemp", with the aircraft spiralling up and down around a spirals a central location approximately 20 km East of the Raman lidar site. In fact, because of the imposed restrictions to air-traffic, aircraft spirals, and consequently sensors' operation, was not possible over the vertical of the lidar measurement site. "WALiTemp" flights took place on 13 September, 02 and 29 October and 05 November 2012, with spiral ascent and descent speeds of approximately 2.5 m/s.

3 Methodology

An appropriate characterization of the space and time variability of aerosol size distribution and microphysical properties is of paramount importance for the understanding of aerosol effect on climate. These most frequently used parameters in this regard are, for example, the volume and surface concentration, the mean and effective radius and the real and imaginary part of the refractive index. This set of microphysical parameters can be used for the determination of the single-scattering albedo, which is a key parameter in the assessment of aerosol radiative forcing in climate studies (Canagaratna et al., 2007).

Retrieval algorithms are used to determine these parameters from multi-wavelength measurements of the particle backscattering and extinction coefficient profiles carried out by the Raman lidars. The main difficulty associated with these algorithms is that the measured optical parameters and the investigated size and microphysical properties are related through non-linear, not analytically solvable, integral equations (Fredholm equations

of the first kind). Numerical solutions of these equations are characterized by strong dependences of the statistical and systematic uncertainties affecting the ingested input data and the missing uniqueness and incompleteness of the solution space. A careful check of the retrieval results is necessary as in fact the inferred solutions may be mathematically correct, but still not reflect the real physical conditions.

In the present research effort, aerosol size distributions and microphysical parameters are obtained from three-wavelength measurements of the particle backscattering and extinction coefficient through a retrieval scheme based on Tikhonov regularization. The retrieval approach assumes particles to be spherical and kernel functions are constructed accordingly. Veselovskii et al. (2002) demonstrated that an input data set including particle backscattering coefficient profiles at 354.7, 532 and 1064 nm ($_{355}(z)$, $_{532}(z)$and $_{1064}(z)$, respectively), and particle extinction coefficient profiles at 354.7 and 532 ($a_{355}(z)$ and $a_{532}(z)$, respectively) is sufficient to determine aerosol size and microphysical parameters, such as number, surface and volume concentration, mean and effective radius and real and imaginary part of the refractive index. Veselovskii et al. (2002) also demonstrated that this is possible only if the overall uncertainty (statistical and/or systematic) affecting particle backscatter profile measurements is smaller than 5 % and the uncertainty affecting particle extinction profile measurements is smaller than 10 %.

4 Results

4.1 Particle backscattering and extinction profiles from BASIL

We focused our attention on the Raman lidar and in-situ measurements carried out on 02 October 2012. Measurements by BASIL started on this day at 16:00 Universal Time Coordinated (UTC) and ended at 24:00 UTC. Figure 1 shows the flying track of the ATR42. At 19:43 the plane took off from the airport of Montpellier to reach an area in the proximity of the observational site in Candillargues. Unfortunately, because of the imposed restrictions to air-traffic, the central location of the aircraft flight pattern, including spirals up and down, was displaced approximately 10-15 km eastward of the lidar measurement site. On this specific flight, ascending-descending spirals were centred on the coordinates Lat: 43 ° 65 N and Long: 4 ° 30 E, 20 km N-NE from the lidar. The maximum radius of these spirals is approximately 5 km. At 19:57 UTC the aircraft reached an altitude of 6 km and began to make descending spirals. Finally, at 22:22 UTC, the plane landed in Montpellier airport. Lidar measurements from BASIL ended at 24:00 UTC.

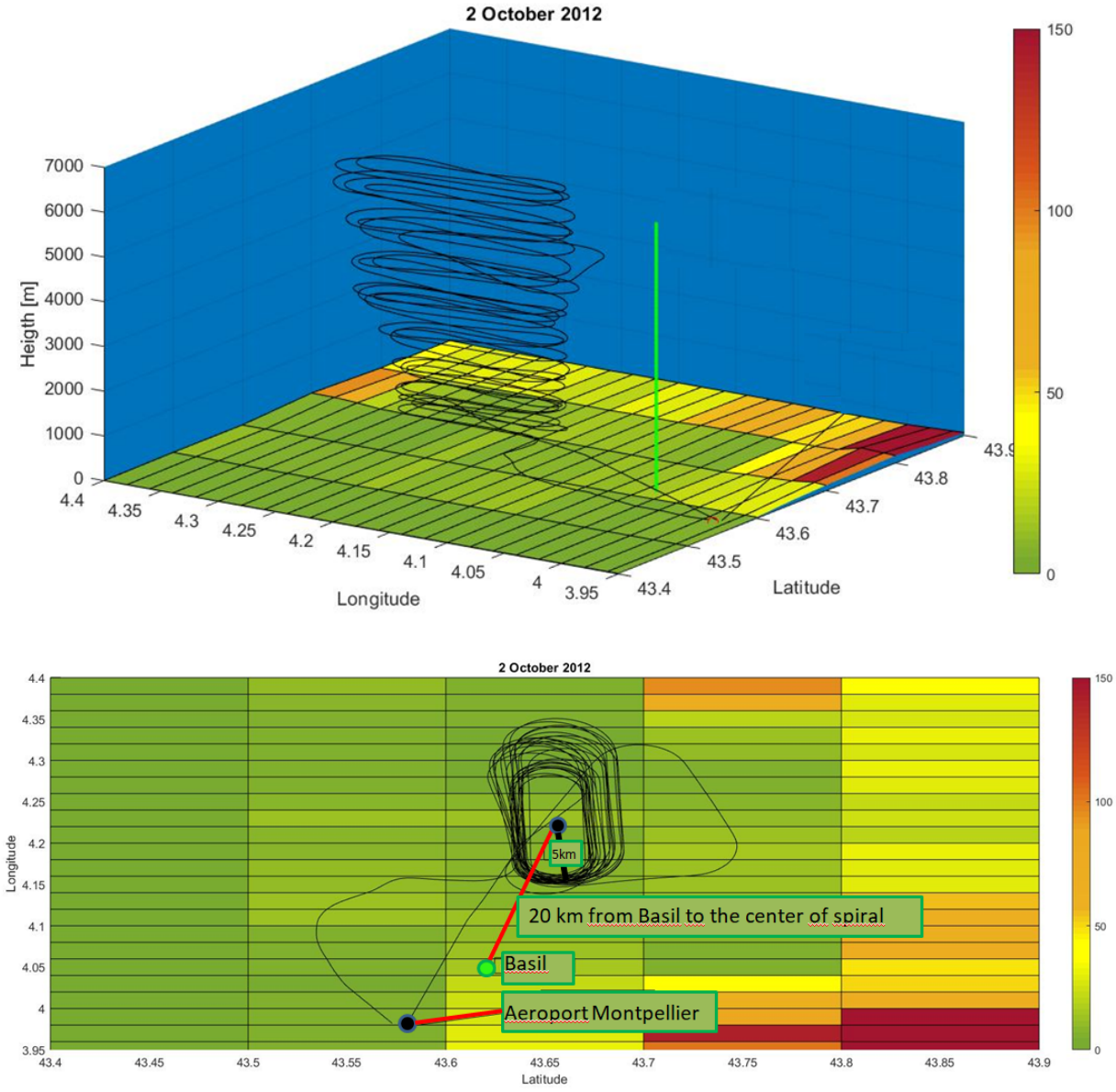

Figure 1: ATR-42 trajectory (black line) from 19:43 to 22:22 UTC. (panel a: tri-dimensional, panel b: horizontal section). The lidar system BASIL is represented as a green line in panel a and as a green dot in panel b.

The colour map in figure 2 shows the time evolution of BASIL measurements of the aerosol backscattering coefficient at 354.7 nm, $_{355}(z)$, covering a ~ 4 h time interval from 19:20 to 23:40 UTC. The figure clearly reveals an aerosol layer extending up to ~ 3 km and a second layer above extending up to ~ 4.5 km.

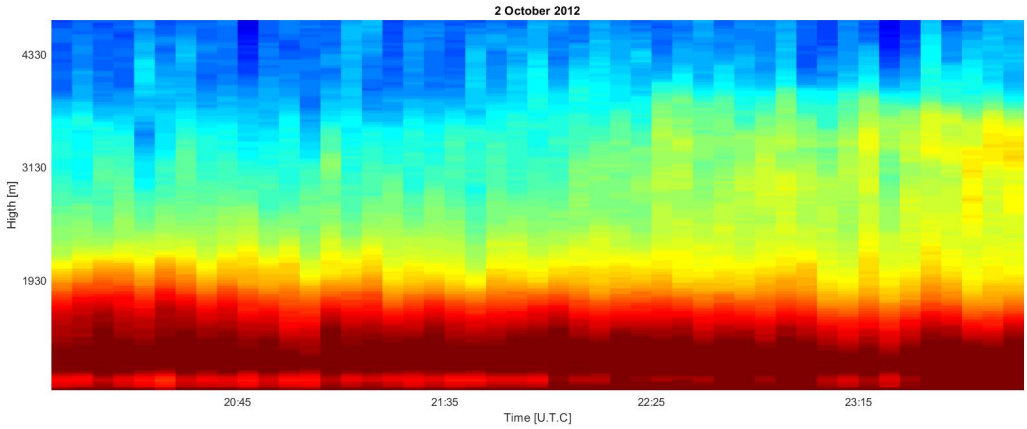

Figure 2: Time evolution of $_{355}(z)$ over the time interval 19:20-23:40 UTC on 02 October 2012.

For the purpose of applying the retrieval scheme and determine particle size distributions and microphysical parameters, we focused over a time interval in the central part of the measurement session, which appears to be characterized by large aerosol concentrations. Additionally, in order to get low enough statistical uncertainties for the retrieval approach to be properly applied, a 2-h integration covering the time interval from 20:00 to 22:00 UTC was considered for both the particle backscattering ($_{355}(z)$, $_{532}(z)$and $_{1064}(z)$) and the extinction coefficient ($a_{355}(z)$ and $a_{532}(z)$) profiles. These profiles, illustrated in figure 3, reveal the presence of a lower aerosol layer, extending up to 3.3 km, and an elevated aerosol layer extending from 3.6 to 4.6 km. The back-trajectory analyses illustrated in the subsequent part of this session reveal that, most probably, the lower aerosol layer originated in a continental area, while the upper layer primary includes aerosols of maritime origin, but an internal mixture with other components encountered during their transport to the observational site.

For the purpose of reducing the statistical uncertainty affecting the different optical parameters, backscattering coefficient profiles were vertically smoothed to achieve a vertical resolution of 150 m, while extinction coefficient profiles were vertically smoothed to achieved a vertical resolution of 300 m. Backscattering coefficient profiles at 355 and 532 were determined through the application of the Raman lidar technique (Ansmann et al. (1992), based on ratioing the elastic signals at these wavelengths with the corresponding N_2 Raman signals at 386.6 and 607 nm, respectively, while the backscattering coefficient profiles at 1064 nm were determined through the application of a Klett-modified method. The extinction coefficient profiles at 354.7 and 532 nm were determined through the approach by Ansmann et al. (1990).

Figure 3: Vertical profiles of the backscattering coefficients $_{355}(z)$, $_{532}(z)$ and $_{1064}(z)$) and the extinction coefficients $a_{355}(z)$ and $a_{532}(z)$.

4.2 Back-trajectory analysis in combination with Aerosol Mass Spectrometer measurements for the assessment of aerosol origin and composition

The NOAA Lagrangian ensemble back-trajectory model HYSPLIT (Draxler and Hess, 1998; Stein et al., 2015; Rolph et al., 2017) is applied to determine the origin of the investigated air masses and establish source–receptor relationships. The Lagrangian trajectory approach involves the calculation of air parcels movement back in time from the receptor site, which yields the back-trajectories of the parcels. Specifically, the ensemble trajectory model starts multiple backward trajectories from the lidar site location at the time of the reported lidar observations. In the HYSPLIT ensemble run, each trajectory is calculated considering an offset of the meteorological data by one meteorological grid point in the horizontal and by 0.01 sigma units in the vertical, which leads to 27 ensemble member trajectories for all-possible 3D (latitude, longitude, altitude) offsets. The consideration of an ensemble approach instead of a single trajectory approach refers to the demonstrated argument (Stohl et al., 2002) that a sufficiently large ensemble of trajectories more correctly represents the behaviour of the ensemble of real air particles. Meteorological data used for the present HYSPLIT runs are taken from the Global Data Assimilation System (GDAS) Reanalysis. Figure 4 shows the 12-days ensemble back-trajectory analysis. Considered back-trajectories are those ending at 2000 m and 4000 m, these being the central altitudes of the aerosol layers observed by BASIL. The analysis ends in Candillargues at 22:00 UTC on 02October 2012 and started at 22:00 UTC on 20 September 2012.

The ensemble back-trajectory analyses reveal that air masses ending at an altitude of 2000 m in Candillargues (figure 4a) originated approximately 10-12 days earlier in continental area in North-Eastern Europe (Poland, Latvia, Lithuania, Estonia and Belarus) and Scandinavia or in North America, and moved over the North Atlantic Ocean for 5-7 days to finally lift up to altitude of 2000 m in the proximity of the Azores Islands (around 28-30 September 2012) and then cross Northern Spain and finally reach the lidar site on 02 October 2012. Ensemble back-trajectory analyses also indicate that the air masses ending at an altitude of 4000 m in Candillargues (figure 4b) originated approximately 10 days earlier over the North Atlantic Ocean and travelled at an altitude between 2 and 3 km for most of the time to finally lift up and overpass Northern Spain 24-48 h before reaching the lidar site. The above ensemble back-trajectory analyses reveal the continental origin of the aerosols in the lower layer and the maritime origin of the aerosols in the upper layer. However air masses observed in both layers experience a long travelling over a marine environment before reaching the observational site, which contributed to their final compositional properties and their external mixture nature, which includes different aerosol components.

In the first lowest 2 km, the Aerosol Mass Spectrometer on board the ATR 42 reveals high concentration values of the main fine aerosols inorganic components, i.e. NO_3, SO_4 and NH_4 (figure 5), these results being compatible with the

aerosol sources identified with the back-trajectory analysis. In this regard it is to be specified that atmospheric NO_3, SO_4 and NH_4 are typically produced through chemical reactions involving particular precursor species such as NOx, SO_2, NH_3 and volatile organic compounds, which can react with O_3 and OH to form secondary aerosols (Guerra et al., 2014; Marais et al., 2016; Kim et al., 2018). These precursor species are mainly of anthropogenic origin and are typically associated with combustion processes. Thus, high concentration of ammonium, sulphate and nitrate are typically found in polluted aerosols of anthropogenic origin, as those sounded in the lower aerosol layer, possibly associated with dust emissions from coal, oil and oil-shale burning power plants and industrial areas in North-Eastern Europe, primarily the Baltic States (Carter, 1994; Yang et al., 2018). Figure 5 also reveals that organic aerosols (OA) represent a large fraction (up to 70%) of the particulate mass in the lowest 2 km. This fraction is possibly formed by primary OA, directly produced by fossil fuel combustion. The measured organic and inorganic aerosol components are also compatible with emissions from biomass burning, as those taking place in North America in the weeks preceding the present observations. The sounded particles are likely to be composed of an external mixture of smoke or dust plus a marine aerosol component. Thus, in the interpretation of the chemical properties and back-trajectory analyses charactering the aerosol particles sounded in the lower layer we consider two possible scenarios, both compatible with chemical and back-trajectory data, i.e. aerosol particles are originally generated i) by forest fires, in North America, or ii) as anthropogenic emissions of particles, in North-Eastern Europe. In both cases, they undergo mixing with marine aerosol during their transport oversea. These hypothesized compositions are also compatible with the particle size distributions and microphysical properties measured by the in-situ sensors and retrieved from the three-wavelength Raman lidar measurements, which are illustrated in the continuation of the paper.

The Aerosol Mass Spectrometer (figure 5) in the altitude interval 3500-4500 m shows increased values of SO_4, which possibly testify gas to particle conversion of biogenic dimethyl-sulphide released from the ocean surface. Increased values of NO_3 are also present in this altitude region, possibly linked to ocean ecosystem productivity. Increased concentrations of secondary organic aerosols (SOA) are also observed, most probably linked to phytoplankton biological activity and its seasonal cycles. Air masses originated over the Atlantic Ocean approximately 10 days earlier than their observation reached the measurements site, overpassing Northern Spain, but without previously overpassing any specific polluted land area, which prevented from the formation of internal/external mixing processes, as possibly observed at other altitudes. As air masses originated over the Atlantic Ocean were transported on the Ocean for most of their way, the sounded aerosol particles in the upper aerosol layer are supposedly either pure marine aerosols or aerosols composed an internal mixture of marine and organic components, the latter being possibly related to ocean phytoplankton biological activity at the sea surface.

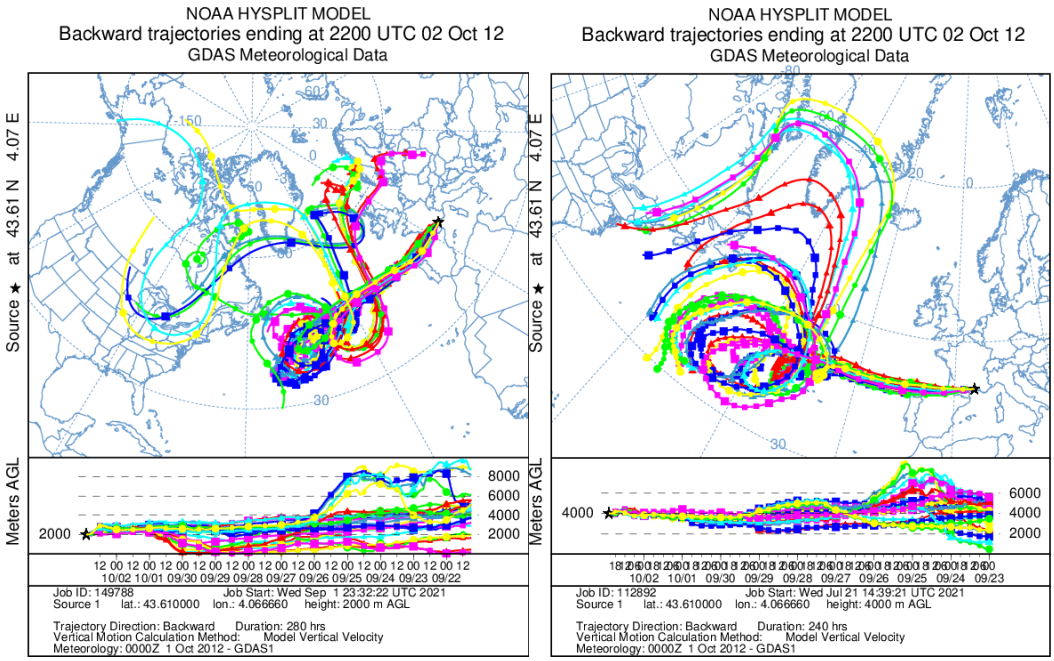

Figure 4: Ensamble back-trajectory analysis. Illustrated back-trajectories end in Candillargues at 2000 m (panel a) and 4000 m (panel b) at 20:00 UTC on 02 October 2012 and started 12 days earlier.

Figure 5: Aerosol Mass Spectrometer measurements. The different chemical species are identified by different colours. The sensor's altitude is represented by the black line.

4.3 Application of the retrieval algorithm

Aerosol dimensional distributions and microphysical properties have been determined from the multi-wavelength Raman lidar data illustrated in figure 3 based on the application of the inversion algorithm illustrated in section 3. Results from these retrievals are illustrated in the following and are compared with simultaneously measurements from in-situ sensors on-board the ATR42.

More specifically, figure 6 illustrates the comparison of BASIL vs. in-situ sensors expressed in terms of volume concentration profile measurements. The two instruments show comparable volume concentration values in both the lower (2-5 mm^3cm^{-3} for the in-situ sensors and 3-4 mm^3cm^{-3} for the Raman lidar) and upper layer (1-3.5 mm^3cm^{-3} for the in-situ sensors and 2-3 mm^3cm^{-3} for the Raman lidar).

The low level peak at 2500 m in the volume concentration measurements from the in-situ sensors is presumably associated with the anthropogenic aerosols transported from industrial areas in North-Eastern Europe (Baltic States) or the biomass-burning aerosols from forest fires in North America, which were

identified in the back-trajectory analysis. On the other hand, the high volume concentration peak value at 4000 m is most likely to be associated with marine aerosols, primarily originated over the North Pacific Ocean, which have been identified in the back-trajectory analysis in the in the altitude interval 3500-4500 m. Retrievals from multi-wavelength Raman lidar measurements allow to properly reproduce the overall structures observed in the volume concentration profile from the in-situ sensors, with a small mismatch (~ 300 m) in the altitude location of two peaks (lower layer peak at 2500 m for the in-situ sensors and at 2200 m for the Raman lidar, upper layer peak at 4000 m for the in-situ sensors and at 4300 m for the Raman lidar). Slight different values in terms of both volume concentration values and location of the peaks are possibly be related to the in situ measurements being point measurements, with a limited degree of vertical integration, while the Raman lidar data are vertically integrated over an interval coincident with its vertical resolution.

Figure 6: Comparison between BASIL and the aircraft in situ sensors, expressed in terms of volume concentration measurements.

Figure 7 illustrates the comparison expressed in terms of effective radius profile measurements between BASIL and the on-board in-situ sensors. Values from the in-situ sensors are in the range 0.35-0.6 m, while values from BASIL are in the range 0.35-0.95 m. BASIL and the in-situ sensors are found to be in good agreement at all altitudes, as in fact values measured by the aircraft sensors are always within the error bar of the corresponding Raman lidar measurements, with the only exception of the data points at ~4 km. Effective radius values in the elevated aerosol layer are slightly larger than in the lower aerosol layer, as in fact pure marine aerosols, including large and giant particles, are typically larger than particles composed of an external mixture of smoke or dust plus an marine aerosol component. The discrepancy observed at 4 km is possibly attributable to the lack in measurement sensitivity of in-situ sensors in the characterization of particle size distributions and microphysical properties in the course mode, as in fact in-situ sensors have a limited response in the coarse mode domain.

Figure 7: Comparison between BASIL and the aircraft in situ sensors, expressed in terms of effective radius.

Comparisons between BASIL and the aircraft sensors were carried out also in terms of particle dimensional distributions. Figure 8 illustrates the aerosol size distribution, expressed in terms of volume concentration, from BASIL at 2200 m and from the in-situ sensors between 1700 and 2300 m. It is to be recalled that the aircraft is characterized by an ascent speed of 150 m per minute, with a temporal integration of the size distribution measurements over a 4-minute interval. Such long integration time is required for in-situ sensors to provide accurate enough volume concentration size distribution measurements. Both sensors reveal the presence of multiple modes. BASIL identifies three distinct modes: a fine mode at 0.2 and two coarse modes at 0.8-1.0 and 3-3.5 m. Small particles (<0.5 m) are presumably representative of an aerosol fraction from combustion processes (biomass burning in the case of aerosols from North America or coal,

oil and oil-shale burning power plants and industrial areas from North-Eastern Europe). The smaller of the two coarse modes, the one centered at 0.8-1.0 m, is probably representative of the carbon fraction component of the sounded marine aerosols, while larger particles (> 2 m) are probably representative of the inorganic component of these aerosols, with the carbonaceous component typically characterized by smaller sizes than the inorganic fraction (O'Dowd et al., 2004; Keene et al., 2007). Coarse aerosols are generally removed from the atmosphere fairly rapidly by sedimentation. However, advection and convective processes can transport these aerosols for long distances (Heald, 2005).

A good agreement between BASIL and the aircraft sensors is found at this altitude. However, a complete separation between the two coarse modes is not captured by the in-situ sensors, whose measurements show the presence of a sort of "merged" mode, with an inflection point around 1 m. In this regard it is to be pointed out that the in-situ sensors have a very limited sensitivity to particle radii larger than 2 m and this may obviously lead to a very limited response to such particle component when present. This translates into the larger of the two coarse modes at 3-3.5 m to generate a fictitious mode in the in-situ measurements around 1.5 m, with volume concentration values (2.5 m ^{3}/cm^3) comparable to those measured at the same altitude by BASIL (2.2 m ^{3}/cm^3), while the smaller of the two coarse modes generates an inflection point around 1 m, characterized by a volume concentration value of 1.2 m ^{3}/cm^3, as opposed to the value of 0.95 m ^{3}/cm^3 measured by BASIL. However, with regard to the fine mode, a very good agreement is present between Raman lidar and in-situ sensors both in terms of radius (0.2 m for both sensors) and volume concentration (1.15 m ^{3}/cm^{3}and 1.20-1.35 m ^{3}/cm^3) values.

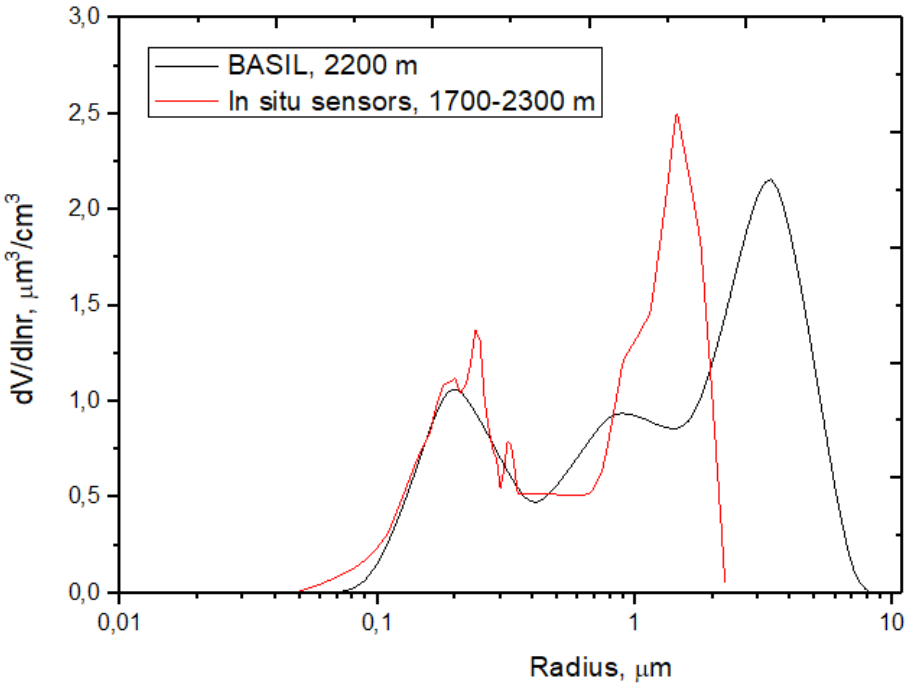

Figure 8: Comparison between BASIL at 2200 m and the aircraft in situ sensors in the height interval 1700-2300 m, expressed in terms of aerosol volume concentration distribution.

Figures 9 shows the aerosol volume concentration distribution as measured by BASIL at 2800 m and by the in-situ sensors in the altitude interval 2400 and 2900 m. The agreement between the two measurements is very good also at this altitude level, with both the Raman lidar and the in-situ sensors identifying the presence of two modes: a fine mode at 0.2 m and a coarse mode at 1.4 m. For what concerns the fine mode, i.e. primarily the aerosol fraction from combustion processes, volume concentration values are very similar to those found at 2200 m, with the Raman lidar and in-situ sensors in very good agreement (1.1 and 1 m ^{3}/cm^3, respectively). For what concerns the coarse marine fraction, only the smaller of the two modes present at 2200 m is left, this mode being characterized by a slightly larger radius (1.4 m) and larger volume concentration values (1.4 m ^{3}/cm^3).

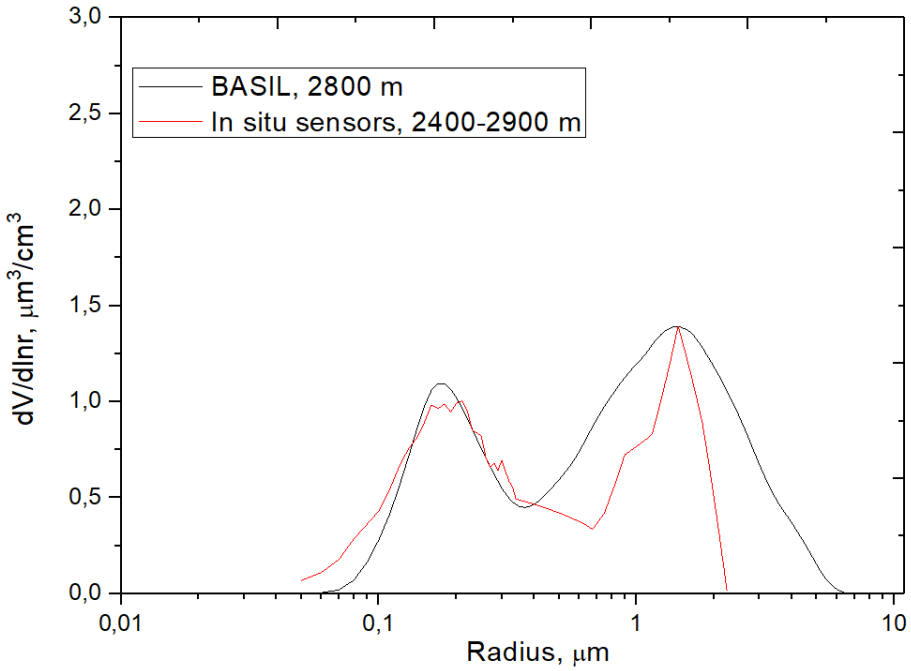

Figure 9: Comparison between BASILs at 2800 m and the aircraft in situ sensors in the height interval 2400-2900 m, expressed in terms of aerosol volume concentration distribution.

Figure 10 shows the aerosol volume concentration distribution as measured by BASIL at 4000 and 4300 m and by the in-situ sensors in the altitude interval 3700 and 4300 m. At these heights, the fine aerosol fraction is found to be considerably reduced. Conversely, the coarse fraction associated with the marine aerosol component becomes predominant. The ensemble back-trajectories indicates that the air masses observed at this heights were originated approximately 10 days earlier over the Atlantic Ocean and, after having traveled the Ocean for 8-9 days, overpassed Spain at considerable high altitudes (~ 4000 m) and therefore were not altered by mixing with any continental or polluted aerosol component.

Again, a very good agreement is found between the Raman lidar and the aircraft sensors, with both instruments properly revealing the presence of the fine and the coarse modes. The fine mode is identified at 0.22 m by BASIL and at 0.18 m by the in-situ sensors, with volume concentration values retrieved by BASIL being 0.25and 0.4 m ^{3}/cm^3 at 4000 and 4300 m, respectively, while volume concentration values measured by the in-situ sensors are up to 0.5 m ^{3}/cm^3. These volume concentration values are approximately 2 to 4 times smaller than those observed at lower altitudes, due to the progressive reduction of the fine

mode fraction with increasing altitudes. This reduction with altitude is also observed in BASIL retrievals, with volume concentration values decreasing from 0.4 m ^{3}/cm^3 at 4000 m to 0.25 m ^{3}/cm^3 at 4300 m.

For what concerns the coarse mode, this is properly identified by BASIL, with volume concentration values being 2.25 and 2.7 m ^{3}/cm^3 at 4000 and 4300 m, respectively. Once again, in-situ sensors do not properly reveal this mode contribution as a result of their limited sensitivity to particles with radii larger than 2 m.

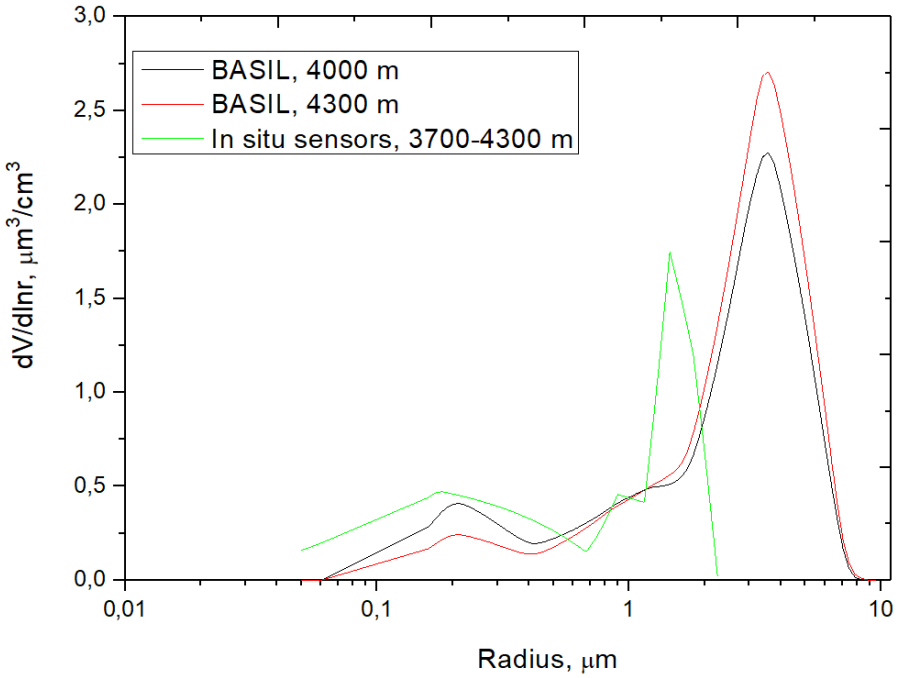

Figure 10: Comparison between BASIL at 4000 and 4300 m and the aircraft in situ sensors in the height interval 3700-4300 m, expressed in terms of aerosol volume concentration distribution.

Other import optical parameters retrieved from the three-wavelength Raman lidar measurements are the real and imaginary part of the particle refractive index. These two quantities are of paramount importance in assessing the scattering and absorbing properties of aerosol particles. More specifically, the real part of the refractive index, m_R, quantifies the light bending within the particle, and consequently its contribution to the scattering, while the imaginary part, m_I, quantifies the light absorption within particle. Figure 11 shown the altitude variability of m_R and m_I as retrieved from BASIL. Values of m_R within the lower aerosol layer are in the range 1.39-1.48, with an average value of 1.44, while in the upper layer m_R varies in the range 1.51-1.54, with an average value of 1.53.

Additionally, values of m_I within the lower aerosol layer are in the range 0.0005-0.00075, with a mean value of 0.0067, while in the upper layer m_R varies in the range 0.011-0.013, with a mean value of 0.00123. In the interpretation of the present results it is to be considered that the retrieval of m_R is characterized by an uncertainty of ± 0.05, while the retrieval of m_I has an uncertainty of ± 50 %. Unfortunately, independent measurements of m_R and m_I from in-situ sensors are not available. However, an indirect estimation of these quantities can be inferred from the compositional information available from the chemical sensor, supported by literature papers.

In principle these two quantities are larger for particle sizes closer to the sounding laser wavelength. For this motivation, the predominantly marine aerosol layer present between 3.6 km and 4.6 km is characterised by small values of both m_R and m_I than those observed in the lower aerosol layer.

Values of m_R retrieved within the lower aerosol layer (1.39-1.48) are compatible with measurements from the chemical sensor, which revealed the abundance in this layer of sulphate and organic carbon, whose values of m_R are 1.43 and 1.53, respectively (Sekiyama et al., 2012), i.e. in the range of those observed in the layer. Retrieved values of m_R are also compatible with the back-trajectory analyses as in fact the aerosol presumably originated in North America from biomass burning or in North-Eastern Europe from coal, oil and oil-shale burning in power plants and industrial areas. In this respect, aerosols from biomass burning have been reported to have m_R values in the range 1.31-1.56 (Sarpong et al., 2020). Furthermore, values of m_R for the submicron and coarse fractions of black carbon particles, which can result from combustion of coal, oil and oil-shale are 1.42-1.45 and 1.50, respectively (Panchenko et al., 2012), also compatible with those observed in the layer.

Values of m_R retrieved within the upper aerosol layer (1.51-1.54) are also compatible with the back-trajectory analyses as in fact aerosol presumably originated over the Atlantic Ocean and were transported on the Ocean for most of their way, with sea salt being a primary component, with reported values of m_R of 1.50 and 1.53 (Sekiyama et al., 2012; Horvath, 1998; Mico et al., 2019), i.e. in the range of those observed in the layer. As previously anticipated, sounded aerosol particles in the upper aerosol layer are supposedly either pure marine aerosols or aerosols composed an internal mixture of marine and organic components, the latter being possibly related to ocean phytoplankton biological activity at the sea surface. In this regard, it has to be recalled that the presence of organic components in the aerosol composition has been identified by the chemical sensor and values of m_R for organic aerosol found in literature (1.53 in Sekiyama et al., 2012, and 1.55 in Zhao et al., 2020) are very close to those found in this aerosol layer.

Values of m_I retrieved within the lower aerosol layer (0.005-0.0075) are compatible with sea salt or water soluble (sulphate, nitrate and ammonium) aerosols (0.006 in Hodzic et al., 2004, and 0.001 in Wang et al., 2021). Values of m_I retrieved within the lower aerosol layer are also compatible with those found

for the submicron and coarse fractions of black carbon particles (0.0075 in Panchenko et al., 2012), which can result from combustion of coal, oil and oil-shale. Observed values of m_I are also compatible with mineral dust particles (0.006 in Mico et al., 2019, and Wang et al., 2021, and 0.0055 in Willoughby et al., 2017). Values of m_I retrieved within the upper aerosol layer (0.011-0.013) are compatible with marine aerosols including an organic component, with values of m_I found in literature for organic and organic carbon aerosols being 0.018 (Wang et al., 2021).

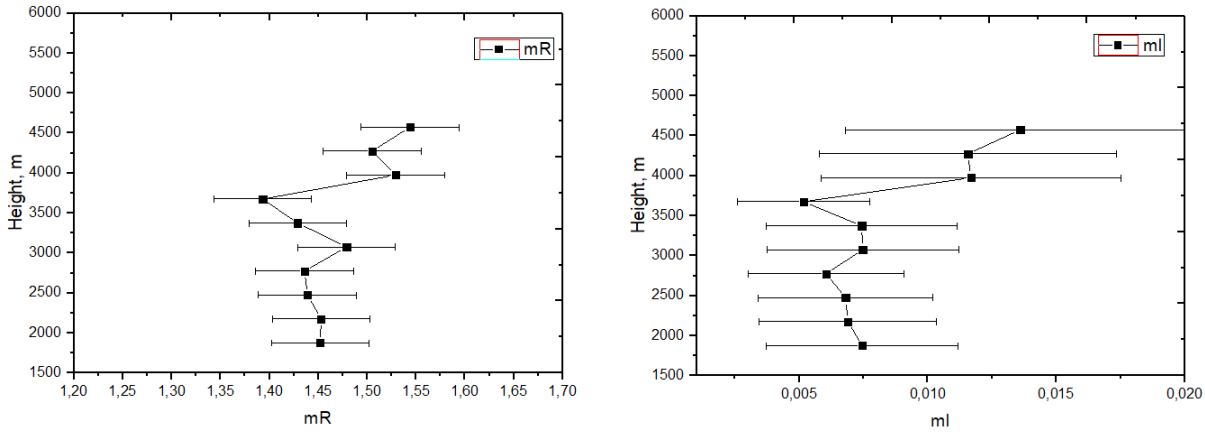

Figure 11: Real (panel a) and imaginary part (panel b) of the particle refractive index.

5 Summary

The paper illustrates a comparison between Raman lidar retrievals and aircraft in-situ sensors' measurements in terms of a variety of aerosol dimensional and microphysical properties, namely size distribution, volume concentration and effective radius. The attention was focused on a case study during HyMeX-SOP1 (02 October 2012), with BASIL measurements indicating the presence of a lower aerosol layer extending from to 3.3 km and an elevated layer extending from 3.6 km to 4.6 km. Results obtained through the retrieval scheme indicate the presence of a size distribution with two particle modes, in both aerosol layers: a fine mode, with a mean radius of approximately 0.2 m, and a coarse mode, with mean radii of 2-4 m. A very good agreement between the lidar and the aircraft sensors is found for all considered parameters. For the purpose of retrieving particle dimensional distributions and microphysical parameters, an algorithm based on Tikhonov regularization was applied to the three-wavelength particle backscattering and extinction coefficient profile measurements from the Raman lidar. In addition to the above mentioned aerosol dimensional and microphysical properties, the retrieval scheme allows to also determine the complex refractive index, which was not measured by the aircraft sensors. The combined use of

Raman lidar retrievals and the in-situ sensors' measurements, in combination with ensemble back-trajectory analyses from the Lagrangian model HYSPLIT and aerosol composition measurements from the Aerosol Mass Spectrometer, allows to properly assess the typologies and origin of the two observed aerosol layers.

Retrievals from three-wavelength Raman lidar measurements highlight the ability of this sensor to characterize the presence of organic aerosols or organic components in mixed aerosol within the free troposphere, especially relying on measurements of the real and imaginary part of the particle refractive index. This measurement capability is particularly important as in fact the concentration of marine organic aerosols in the free troposphere are often significantly underestimated by models (Kim et al., 2018) and a better quantification of their concentrations and composition, in combination with a more accurate assessment of their sources and transportation paths, is fundamental in a variety of environmental issues ranging from radiative balance and air quality.

Acknowlegments

Wind Profiler dataset were collected in the frame of the HyMeX program, sponsored by Grants MISTRALS/HyMeX and ANR-11-BS56-0005 IODA-MED project (contact person: Frédérique Saïd, Université Toulouse-Laboratoire d'Aérologie, Toulouse, France). This work was supported by the Italian Ministry for Education, University and Research under the Grants OT4CLIMA and FISR2019-CONCERNING, and by the Italian Space Agency under the Grants As-ATLAS and CALIGOLA. Lidar retrieval algorithms were developed thanks to the support by Russian Science Foundation (project 21-17-00114). The dataset used in the present research effort and the corresponding metadata are archived in the open public data repository HyMeX database, freely accessible through the link http://mistrals.sedoo.fr/HyMeX/.

Reference

Albrecht, B. A. (1989), Aerosols, cloud microphysics, and fractional cloudiness. *Science*, 245(4923), 1227–1230.

Andreae, M. O., Elbert, W., & de Mora, S. J. (1995), Biogenic sulfur emissions and aerosols over the tropical South Atlantic. 3. Atmospheric dimethylsulfide, aerosols and cloud condensation nuclei. *Journal of Geophysical Research*, *100*(6), 335–356.

Andrews, E., Saxena, P., Musarra, S., Hildemann, L.M., Koutrakis, P., McMurry, P.H., Olmez, I., & White, W.H. (2000) " Concentration and Composition of Atmospheric Aerosols from the 1995 SEAVS Experiment and a Review of the Closure between Chemical and Gravimetric Measurements" , *Journal of the Air & Waste Management Association*, 50:5, 648-664, doi: 10.1080/10473289.2000.10464116.

Ansmann, A., Riebesell, M., Weitkamp, C. (1990), Measurement of atmospheric aerosol extinction profiles with a Raman lidar*," Optics Letters, 15*, 746-748.

Ansmann, A., Wandinger, U., Riebesell, M., Weitkamp, C., and Michaelis, W. (1992), Independent measurement of extinction and backscatter profiles in cirrus clouds by using a combined Raman elastic-backscatter lidar. *Applied Optics*, *31*, 7113-7131.

Bauer, S. E., Koch, D., Unger, N., Metzger, S. M., Shindell, D. T., & Streets, D. G. (2007), Nitrate aerosols today and in 2030: a global simulation including aerosols and tropospheric ozone. *Atmospheric Chemistry and Physics* , 7, 5043–5059.

Bassett, M., & Seinfeld, J. H. (1984), Atmospheric equilibrium model of sulfate and nitrate aerosols-II. Particle size analysis. *Atmospheric Environment*, 18, 1163-1170.

Bonsang, B., Polle, C., & Lambert, G. (1992), "Evidence for marine production of isoprene. *Geophysical Research Letters*, *19*(11), 1129–1132.

Boucher, O., Randall, D., P. Artaxo, C. Bretherton, G. Feingold, P. Forster, V.-M. Kerminen, Y. Kondo, H. Liao, U. Lohmann, P. Rasch, S.K. Satheesh, S. Sherwood, B. Stevens, and X.Y. Zhang, (2013), Clouds and aerosols. In Climate Change 2013: The Physical Science Basis. Contribution of Working Group I to the *Fifth Assessment Report of the Intergovernmental Panel on Climate Change*. T.F. Stocker, D. Qin, G.-K. Plattner, M. Tignor, S.K. Allen, J. Doschung, A. Nauels, Y. Xia, V. Bex, and P.M. Midgley, Eds. Cambridge University Press, pp. 571-657, doi:10.1017/CBO9781107415324.016.

Canagaratna, M. R., J. T. Jayne, J. L. Jimenez, J. D. Allan, M. R. Alfarra, Q. Zhang, T.B. Onasch, F. Drewnick, H. Coe, A. Middlebrook, A. Delia, L.R. Williams, A. M. Trimborn, M.J. Northway, P.F. De Carlo,C.E. Kolb, P. Davidovits, D.R. Worsnop (2007), Chemical and microphysical characterization of ambient aerosols with the aerodyne aerosol mass spectrometer. *Mass Spectrom Rev.*, *26*(2), 185-222, doi: 10.1002/mas.20115. PMID: 17230437.

Carter, W. P. (1994), Development of ozone reactivity scales for volatile organic compounds. *Air Waste*, *44*, 881–899. https://doi.org/10.1080/1073161X.1994.10467290.

Charlson, R. J., Schwartz, S. E., Hales, J. M., et al. (1992), Climate forcing by anthropogenic aerosols. *Science*, *255*(5043), 423–430.

Crumeyrolle, S., Manninen, H. E., Sellegri, K., Roberts, G., Gomes, L., Kulmala, M., Weigel, R., Laj, P., and Schwarzenboeck, A. (2010) "New particle formation events measured on board the ATR-42 aircraft during the EUCAARI campaign " Atmos. Chem. Phys., 10, 6721–6735, 2010 https://doi.org/10.5194/acp-10-6721-2010.

De Rosa , B., Di Girolamo, P., Summa, D. (2018a), Characterization of atmospheric thermodynamic variables by Raman lidar in the frame of the International Network for the Detection of Atmospheric Composition Change – NDACC" *EPJ Web Conf.,* 176 (2018) 04010, DOI: https: //doi.org/10.1051/epjconf/201817604010.

De Rosa, B., P. Di Girolamo, D. Summa, C. Flamant, O. Bousquet, M. Cacciani, D. Stelitano (2018b), Temperature inter-comparison effort in the framework of Hydrological Cycle in the Mediterranean Experiment – Special Observation Period (HyMeX-SOP1) *EPJ Web Conf.*, 176 (2018) 08010 DOI: https://doi.org/10.1051/epjconf/201817608010.

De Rosa, B., Di Girolamo, P., Summa, D. (2020), Temperature and water vapour measurements in the framework of the Network for the Detection of Atmospheric Composition Change (NDACC), *Atmos. Meas. Tech.*, *13*, 405–427, https://doi.org/10.5194/amt-13-405-2020.

Di Girolamo, P., Gagliardi, R. V., Pappalardo, G., Spinelli, N., Velotta, R., Berardi, V. (1995), Two wavelength Lidar analysis of stratospheric aerosol size distribution. *Journal of Aerosol Science*, *26*, 989-1001, ISSN: 0021-8502, doi: 10.1016/0021-8502(95)00025-8,.

Di Girolamo, P., Ambrico, P. F., Amodeo, A., Boselli, A., Pappalardo, G., Spinelli, N. (1999), Aerosol observations by Lidar in the Nocturnal Boundary Layer. *Applied Optics*, *38*, 4585-4595, ISSN: 0003-6935, doi: 10.1364/AO.38.004585.

Di Girolamo, P., Marchese, R., Whiteman, D. N., and Demoz, B. B. (2004), Rotational Raman Lidar measurements of atmospheric temperature in the UV, *Geophysical Research Letters*, *31*, L01106, doi:10.1029/2003GL018342.

Di Girolamo, P., Behrendt, A., & Wulfmeyer, V. (2006), Spaceborne profiling of atmospheric temperature and particle extinction with pure rotational Raman Lidar and of relative humidity in combination with differential absorption Lidar: performance simulations. *Applied Optics*, *45*, 2474-2494, ISSN: 0003-6935, doi: 10.1364/AO.45.002474.

Di Girolamo, P., A. Behrendt, C. Kiemle, V. Wulfmeyer, H. Bauer, D. Summa,

A. Dörnbrack, G. Ehret (2008), Simulation of satellite water vapourlidar measurements: Performance assessment under real atmospheric conditions. *Remote Sensing of Environment*, *112*, 1552-1568, ISSN: 0034-4257, doi: 10.1016/j.rse.2007.08.008.

Di Girolamo, P., Summa, D., Ferretti, R. (2009). Multiparameter Raman Lidar Measurements for the Characterization of a Dry Stratospheric Intrusion Event. *Journal of Atmospheric and Oceanic Technology*, *26*, 1742-1762, ISSN: 0739-0572, doi: 10.1175/2009JTECHA1253.1.

Di Girolamo, P., D. Summa, M. Cacciani, E. G. Norton, G. Peters, Y. Dufournet (2012a), Lidar and radar measurements of the melting layer: observations of dark and bright band phenomena. *Atmospheric Chemistry and Physics*, *12*, 4143-4157, ISSN: 1680-7316, doi: 10.5194/acp-12-4143-2012,.

Di Girolamo, P. et al., (2012b), Raman lidar observations of a Saharan dust outbreak event: Characterization of the dust optical properties and determination of particle size and microphysical parameters" *Atmospheric Environment*, *50*, 66-78.

Di Girolamo, P., Scoccione, A., Cacciani, M., Summa, D., De Rosa, B., Schween, J. H. (2018), Clear-air lidar dark band. *Atmos. Chem. Phys.*, *18*, 4885–4896, 2018 https://doi.org/10.5194/acp-18-4885-2018.

Di Girolamo, P., B. De Rosa, C. Flamant, D. Summa, O. Bousquet, P. Chazette, J. Totems, M. Cacciani, 2020 "Water vapor mixing ratio and temperature intercomparison results in the framework of the Hydrological Cycle in the Mediterranean Experiment—Special Observation Period 1, *Bulletin of Atmospheric Science and Technology* (2020) 1:113–153 https://doi.org/10.1007/s42865-020-00008-3.

Draxler, R. R. and Hess, G. D. (1998), An overview of the HYSPLIT_4 modeling system for trajectories, dispersion and deposition, *Aust. Meteorol. Mag.*, 47, 295–308.

Drewnick , F., S. S. Hings, P. DeCarlo , J. T. Jayne , M. Gonin, K. Fuhrer , S. Weimer , J. L. Jimenez, K. L. Demerjian, S. Borrmann & D. R. Worsnop (2005), A New Time-of-Flight Aerosol Mass Spectrometer (TOF-AMS)—Instrument Description and First Field Deployment", *Aerosol Science and Technology*, 39:7, 637-658, DOI: 10.1080/02786820500182040.

Elterman, L. (1966), Aerosol Measurements in the Troposphere and Stratosphere. *Applied Optics 5*, 1769-1776.

Facchini, M. C., Rinaldi, M., Decesari, S., et al. (2008), Primary submicron marine aerosol dominated by insoluble organic colloids and aggregates. *Geophysical*

Research Letters, *35*(17), Article ID L17814.

Falkowski, P. G., Kim, Y., Kolber, Z., Wilson, C., Wirick, C., and Cess, R. (1992), Natural versus anthropogenic factors affecting low-level cloud albedo over the North Atlantic. *Science*, *256*(5061), 1311–1313.

Fernald, F. G. (1984), Analysis of atmospheric lidar observations: some comments. *Applied Optics 23*, 652-653**.**

Fiocco, G., & Grams, G. (1964), Observations of the Aerosol Layer at 20 km by Optical Radar. *Journal of the Atmospheric Sciences*, *21*, 323-324.

Fraser, M.P., Lakshmanan, K., Fritz, S.G., Ubanwa (2002), Variation in composition of fine particulate emissions from heavy-duty diesel vehicles. *Journal of Geophysical Research Atmospheres* 107 (D21), in press, doi:10.1029/2001JD000558.

Freudenthaler, V., Esselborn, M., Wiegner, M., Heese, B., Tesche, M., Ansmann, A., Müller, D., Althausen, D., Wirth, M., Fix, A., Ehret, G., Knippertz, P., Toledano, C., Gasteiger, J., Garhammer, M. And Seefeldner, M. (2009), Depolarization ratio profiling at several wavelengths in pure Saharan dust during SAMUM 2006. *Tellus* B, 61: 165-179. https://doi.org/10.1111/j.1600-0889.2008.00396.x.

Gard, E. E, Kleeman, M. J., Gross, D. S, Hughes, L. S. et al. (1998), Direct Observation of Heterogeneous Chemistry in the Atmosphere" *Science, 279*(5354), 1184-1187.

Guerra, S.A, Olsen. S.R, Anderson. J.J. (2014) Evaluation of the SO2 and NOx offset ratio method to account for secondary PM2.5 formation. *J. Air Waste Manag. Assoc.*, *64*(3):265–271. https://doi.org/10.1080/10962247.2013.852636.

Heald, C. L., Daniel J. Jacob,Rokjin J. Park,Lynn M. Russell,Barry J. Huebert,John H. Seinfeld,Hong Liao,Rodney J. Weber, (2005), A large organic aerosol source in the free troposphere missing from current models, *Geophysical Research Letters*, *32*, L18809.

Heim, M., Benjamin J. Mullins, B. J., Umhauera, H., Kaspera, G. (2008), Performance evaluation of three optical particle counters with an efficient "multimodal" calibration method. *Journal of Aerosol* Science, *39*(12), 1019-1031,ISSN 0021-8502,https://doi.org/10.1016/j.jaerosci.2008.07.006.

Hodzic, A., H. Chepfer R. Vautard P. Chazette M. Beekmann B. Bessagnet

B. Chatenet J. Cuesta P. Drobinski P. Goloub M. Haeffelin Y. Morille (2004), Comparison of aerosol chemistry transport model simulations with lidar and Sun photometer observations at a site near Paris, *J. Geophys. Res.*, *109*, D23201, doi:10.1029/2004JD004735.

Horvath, H. (1998), Influence of atmospheric aerosols upon the global radiation balance, in *Atmospheric Particles*, *5*, 543–596, edited by R. M. Harrison and R. E. van Grieken (Wiley-InterScience, New York).

IPCC (2007), Summary for policy makers, in *Climate Change 2007: The Physical Science Basis. Contribution of Working Group I to the Fourth Assessment Report of the Intergovernmental Panel on Climate Change*, S. Solomon, D. Qin, and M. Manning, Eds., Cambridge University Press, Cambridge, UK.

Keene, W. C., Maring, H., Maben, J. R., et al., (2007), Chemical and physical characteristics of nascent aerosols produced by bursting bubbles at a model air-sea interface. *Journal of Geophysical Research D*, *112*(21), Article ID D21202.

Kim, H., Zhang, Q., Heo, J. (2018), Influence of intense secondary aerosol formation and long-range transport on aerosol chemistry and properties in the Seoul Metropolitan Area during spring time: results from KORUSAQ. *Atmos. Chem. Phys.*, 18:7149–7168. https://doi.org/10.5194/acp-18-7149-2018.

Klett, J. D. (1981), Stable analytical inversion solution for processing lidar returns. *Applied Optics 20*, 211-220.

Klett, J. D. (1985), Lidar inversion with variable backscatter/extinction ratios. *Applied Optics 24*, 1638-1643.

Leck, C., & Bigg E. K. (2005a), Source and evolution of the marine aerosol—a new perspective. *Geophysical Research Letters*, *32*(19), Article ID L19803, 1–4.

Leck, C., & Bigg E. K. (2005b), Biogenic particles in the surface microlayer and overlaying atmosphere in the central Arctic Ocean during summer. *Tellus, Series B*, *57*(4), 305–316.

Lelieveld, J., Roelofs, G.–J., Ganzeveld, L., Feichter, J., & Rodhe, H. (1997), Terrestrial sources and distribution of atmospheric sulphur. *Phil. Trans. R. Soc. Lond.* B352149–158.

Li-Jones, X., and Prospero, J. M. (1998), Variations in the size distribution of non-sea-salt sulfate aerosol in the marine boundary layer at Barbados: Impact of African dust, *J. Geophys. Res.*, *103*(D13), 16073– 16084, doi:10.1029/98JD00883.

Mansfield, T., Hamilton, R., Ellis, B. et al. (1991), Diesel particulate emissions and the implications for the soiling of buildings. *Environmentalist*, vol. 11, pp.243–254. https://doi.org/10.1007/BF01266558.

Marais, E. A., Jacob, D. J, Jimenez, J. L., Campuzano-Jost, P., Day, D. A., Hu, W., Krechmer, J., Zhu L, Kim PS, Miller CC,Fisher JA, Travis K, Yu K, Hanisco TF, Wolfe GM, Arkinson HL, Pye HOT, Froyd, K. D., Liao, J., Mc Neill, V.F. (2016), Aqueous-phase mechanism for secondary organic aerosol formation from isoprene: application tothe southeast United States and co-benefit of SO2 emission controls. *Atmos. Chem. Phys.*, *16*, 1603–1618.https://doi.org/10.5194/acp-16-1603-2016.

Mico, S., A. Deda, E. Tsaousi, M. Alushllari, and P. Pomonis (2019), Complex Refractive Index of Aerosol Samples, *Women in Physics*, AIP Conf. Proc. 2109, 060002-1–060002-4; https://doi.org/10.1063/1.5110120.

Müller, D., Wandinger, U., & Ansmann, A. (1999), Microphysical particle parameters from extinction and backscatter lidar data by inversion with regularization: simulation. *Applied Optics, 38*, 2358-2368.

Müller, D., Ansmann, A., Mattis, I., Tesche, M., Wandinger, U., Althausen, D., Pisani, G. (2007), Aerosol-type-dependent lidar ratios observed with Raman lidar. *Journal of Geophysical Research, 112* D16202.

Murphy , D. M., & Thomson, D. S. (1997), Bromine, iodine, and chlorine in single aerosol particles at Cape Grim. *Geophysical Research Letters*, *24*(24), 3197-3200.

O'Dowd, C. D., Facchini, M. C., Cavalli F., et al. (2004), Biogenically driven organic contribution to marine aerosol. *Nature*, *431*(7009), 676–680.

Panchenko, M. V., T. B. Zhuravleva, S. A. Terpugova, V. V. Polkin, and V. S. Kozlov (2012), An empirical model of optical and radiative characteristics of the tropospheric aerosol over West Siberia in summer, *Atmos. Meas. Tech.*, 5, 1513–1527, www.atmos-meas-tech.net/5/1513/2012/, doi:10.5194/amt-5-1513-2012.

Pérez-Ramírez , D., D. N.Whiteman, I.Veselovskii, P.Colarcof, M. Korenski , A. Silva (2019), Retrievals of aerosol single scattering albedo by multiwavelength lidar measurements: Evaluations with NASA Langley HSRL-2 during discover-AQ field campaigns. *Remote Sensivg of Enviromental*, *222*, 144-164.

Rap, A. (2013), Natural aerosol direct and indirect radiative effects. *Geophysical Research Letters*, 40, 3297-3301.

Rogge, W. F., M. A. Mazurek, Lynn M. Hildemann, Glen R. Cass, Bernd Simoneit, R.T. (1993), Quantification of urban organic aerosols at a molecular level: Identification, abundance and seasonal variation, *Atmospheric Environment*. Part A. General Topics, *27*(8), 1309-1330, ISSN 0960-1686, https://doi.org/10.1016/0960-1686(93)90257-Y.

Rogge, W. F., Lynn M. Hildemann, Monica A. Mazurek, Glen R. Cass, Bernd R. T. (1993), Simoneit,Sources of Fine Organic Aerosol. 2. Noncatalyst and Catalyst-Equipped Automobiles and Heavy-Duty Diesel Trucks, *Environ. Sci. Techno*, 27, 636-651.

Rolph, G., Stein, A., and Stunder, B. (2017): Real-time Environmental Applications and Display sYstem: READY, *Environ. Modell. Softw.*, *95*, 210–228, https://doi.org/10.1016/j.envsoft.2017.06.025.

Sarpong, E., Smith, D., Pokhrel, R., Fiddler, M. N., Bililign, S. (2020), Refractive Indices of Biomass Burning Aerosols Obtained from African Biomass Fuels Using RDG Approximation. *Atmosphere*, *11*, 62. https://doi.org/10.3390/atmos11010062.

Sekiyama, T. T., Tanaka, T. Y., and Miyoshi, T. (2012), A simulation study of the ensemble-based data assimilation of satellite-borne lidar aerosol observations, *Geosci. Model Dev. Discuss.*, 5, 1877–1947, https://doi.org/10.5194/gmdd-5-1877-2012.

Stein, A. F., Draxler, R. R., Rolph, G. D., Stunder, B. J. B., Cohen, M. D., and Ngan, F. (2015), NOAA's HYSPLIT Atmospheric Transport and Dispersion

Modeling System, *Bulletin of the American Meteorological Society*, *96*, 2059–2077, https://doi.org/10.1175/BAMS-D-14-00110.1.

Stohl, A., S. Eckhardt, C. Forster, P. James, N. Spichtinger, P. Seibert (2002), A replacement for simple back trajectory calculations in the interpretation of atmospheric trace substance measurements, *Atmospheric Environment*, *36*, 4635–4648.

Sullivan, A. P., May, A. A., Lee, T., McMeeking, G. R., Kreidenweis, S. M., Akagi, S. K., Yokelson, R. J., Urbanski, S. P., and Collett Jr., J. L.: Airborne characterization of smoke marker ratios from prescribed burning, Atmos. Chem. Phys., 14, 10535–10545, https://doi.org/10.5194/acp-14-10535-2014, 2014.

Summa, D., P. Di Girolamo, C. Flamant, B. De Rosa, M. Cacciani, D. Stelitano (2018), Water vapour inter-comparison effort in the framework of the hydrological cycle in the mediterranean experiment – special observation period (hymex-sop1) EPJ Web Conf., 176 (2018) 08016.

Turpin, B. J., Saxena, P., Andrews, E. (2000), Measuring and simulating particulate organics in the atmosphere: problems and prospects " *Atmospheric Environment*, *34*(18), 2983-3013, ISSN 1352-2310, https://doi.org/10.1016/S1352-2310(99)00501-4.

Twomey, S. (1977). The Influence of Pollution on the Shortwave Albedo of Clouds, Journal of Atmospheric Sciences, 34(7), 1149-1152.

Veselovskii, I., Kolgotin, A., Griaznov, V., Müller, D., Wandinger, U., and Whiteman, D. (2002), Inversion with regularization for the retrieval oftropospheric aerosol parameters from multi-wavelength lidar sounding, *Applied Optics*, 41, 3685–3699.

Veselovskii et al. 2010, "Application of randomly oriented spheroids for retrieval of dust particle parameters from multiwavelength lidar measurements " *Journal of Geophysical Research* vol. 115, D21203, doi:10.1029/2010JD014139.

Veselovskii I., O. Dubovik, A. Kolgotin, T. Lapyonok, P. Di Girolamo, D. Summa, D. N. Whiteman, M. Mishchenko, D. Tanré (2010). Application of randomly oriented spheroids for retrieval of dust particle parameters from multiwavelength Lidar measurements. *Journal of Geophysical Research*, *115*, ISSN: 0148-0227, doi: 10.1029/2010JD014139.

Veselovskii, I., O. Dubovik, A. Kolgotin, M. Korenskiy, D. N. Whiteman, K. Allakhverdiev, and F. Huseyinoglu (2012),Linear estimation of particle bulk parameters from multi-wavelength lidar measurements, *Atmos. Meas. Tech., 5*, 1135–1145, doi:10.5194/amt-5-1135-2012.

Veselovskii I, Goloub P, Podvin T, et al. (2018) Characterization of smoke and dust episode over West Africa: comparison of MERRA-2 modeling with multiwavelength Mie-Raman lidar observations. Atmospheric Measurement Techniques. Mar;11(2):949-969. DOI: 10.5194/amt-11-949-2018. PMID: 32699562; PMCID: PMC7375260.

Wang, Y. (2020), Impacts of long-range transport of aerosols on marine-boundary-layer clouds in the eastern North Atlantic. *Atmos. Chem. Phys.*, *20*, 14741–14755, https://doi.org/10.5194/acp-20-14741-2020.

Wang, S., S. Crumeyrolle, W. Zhao, X. Xu, B. Fang, Y. Derimian, C. Chen, W. Chen, W. Zhang, Y. Huang, X. Deng, Y. Tong (2021), Real-time retrieval of aerosol chemical composition using effective density and the imaginary part of complex refractive index, *Atmospheric Environment*, *245*, 117959, ISSN 1352-2310, https://doi.org/10.1016/j.atmosenv.2020.117959.

Willoughby, R. E., M. I. Cotterell, H. Lin, A. J. Orr-Ewing and J. P. Reid (2017), Measurements of the Imaginary Component of the Refractive Index of Weakly Absorbing Single Aerosol Particles. *J. Phys. Chem. A*, *121*, 5700−5710, doi: 10.1021/acs.jpca.7b05418.

Wulfmeyer, V., Bauer, H., Di Girolamo, P., Serio, C. (2005), Comparison of active and passive water vapor remote sensing from space: An analysis based on the simulated performance of IASI and space borne differential absorption lidar. *Remote Sensing of Environment, 95*, 211-230.

Yang, W., Li, J., Wang, M., Sun, Y., Wang, Z. (2018), A case study of investigating secondary organic aerosol formation pathways in Beijing using an observation-based SOA box model. *Aerosol. Air Qual. Res.*, *18*, 1606–1616. https://doi.org/10.4209/aaqr.2017.10.0415.

Zhang, D., G.-Y. Shi, Iwasaka, Y., Hu, M. (2000), Mixture of sulfate and nitrate in coastal atmospheric aerosols: Individual particle studies in Qingdao (36°04'N, 120°21'E), China. *Atmospheric Environment, 34*, 2669-2679.

Zhao, D., Yin, Y., Zhang, M., Wang, H., Lu, C., Yuan, L., Shi, S. (2020), The Optical Properties of Aerosols at the Summit of Mount Tai in May and June and the Retrieval of the Complex Refractive Index. *Atmosphere*, *11*, 655. https://doi.org/10.3390/atmos11060655.

Zorn, S. R., Drewnick, F., Schott, M., Hoffmann, T., & Borrmann, S. (2008), Characterization of the South Atlantic marine boundary layer aerosol using an aerodyne aerosol mass spectrometer. *Atmospheric Chemistry and Physics*, *8*(16), 4711–4728.